Research Article

Journal of Robotics and Automation Research

Bearing Fault Diagnosis Based On Improved Cepstrum

Jian Wang and Yongjian Sun*

School of Electrical Engineering, University of Jinan, Jinan, Shandong, China

***Corresponding author**
Yongjian Sun, School of Electrical Engineering, University of Jinan, Jinan, Shandong, China.

Submitted: 22 July 2021; **Accepted:** 28 July 2021; **Published:** 10 Aug 2021

Citation: *Jian Wang and Yongjian Sun. (2021). Gearbox Fault Feature Extraction and Diagnosis. J Robot Auto Res, 2(2), 19-23.*

Abstract

Rolling bearing is widely used in various mechanical equipment, which affects the performance and safety of the equipment. In order to ensure the normal operation of the equipment, a new method based on improved cepstrum for bearing fault diagnosis is proposed. In the cepstrum peaks, the largest four peaks are extracted, then the four peaks are improved to complete the feature extraction of bearing fault. Simulation experiment was carried out to verify the accuracy of the proposed method. The experimental results show that the accuracy is up to 92.44%, which has achieved high accuracy.

Keywords: Rolling Bearing, Feature Extraction, Improved Cepstrum, Fault Diagnosis

Introduction

Rolling bearing is widely used in industrial rotating machinery. The normal operation of rolling bearing is related to the safety of the whole industrial system, so it is very important to extract the feature and diagnose the fault of rolling bearing. In the field of rolling bearing fault diagnosis, many fault diagnosis methods have been proposed and achieved good results. Karatoprak proposed an improved Empirical Mode Decomposition (EMD) method named MEMD [1]. The results showed that MEMD method was better than EMD on bearing fault feature extraction. Zheng also proposed an improve method named mean-optimized mode decomposition (MOMD) method to realize the bearing fault diagnosis [2]. Experimental results showed that MOMD method has better effect than EMD. A novel method based on the combination of complete ensemble EMD with adaptive noise (CEEMDAN) is proposed by He [3]. The results showed that this method was effective and correct. Cai proposed a novel method by cooperating empirical mode decomposition (EMD) with genetic neural network adaptive boosting (GNN-Ada Boost) [4]. Experimental results showed that GNN-AdaBoost was more effective than GNN. Wavelet packet is also used to help realize the bearing fault diagnosis. Wang proposed a supervised sparsity-based wavelet feature (SSWF) [5]. Wavelet packet transform (WPT) is combined with the sparse coding. An enhanced Frequency Band Entropy (EFBE) adopting WPT as the filter of FBE was proposed by Li [6]. The fault feature frequency is extracted by combining the filtered signal and the envelope power spectrum. Wan proposed a diagnosis method named FERgram, which is based on the fault energy ratio (FER) and the maximal overlap discrete wavelet packet transform (MODWPT) [7]. A novel method based on cooperation of Resonance-based Sparse Signal Decomposition (RSSD) and Wavelet Transform (WT) was proposed by Chen [8]. The fault signal of is decomposed by RSSD. Huang proposed a novel method based on orthogonal wavelet packet decomposition and Gaussian Mixture Model-Hidden Markov Model (GMM-HMM). The results verified the accuracy of the GMM-HMM method [9]. Zhang proposed a novel method by using wavelet packet energy (WPE) and fast kurtogram (FK) [10]. Experimental results showed that the fault feature could be extracted more effectively than the traditional FK method. Wei used envelope entropy as objective function for the whale optimization algorithm (WOA) [11]. Experimental results showed that the method was more effective compared with wavelet packet decomposition.

In this paper, a new method based on improved cepstrum for bearing fault diagnosis is proposed. The second section presents the data sources. In the third section, the primitive cepstrum and the improved cepstrum are introduced. In the fourth section, a simulation experiment is designed and carried out to verify the accuracy of the method. Finally, a conclusion is made in the fifth section.

Data Sources and Data Processing

Data Sources

In this paper, the bearing data of Western Reserve University in USA are selected. The experimental setup of Western Reserve University is shown in Figure 1.

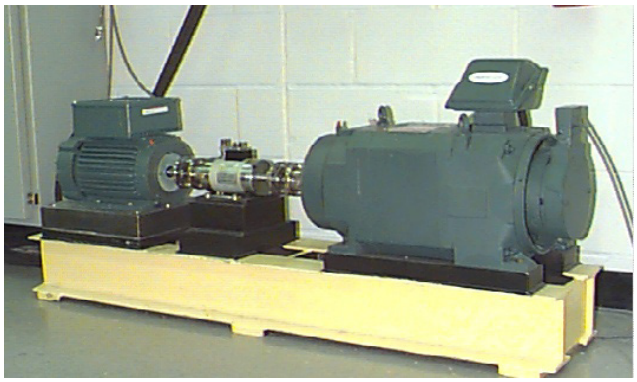

Figure 1: Bearing test bed of Western Reserve University

As shown in Figure 1, the test bed is made up of a motor, a torque sensor and a power tester. The test bed has a normal SKF6205 bearing and a faulty SKF6205 bearing, And the sampling frequency is 12 KHz. In order to complete the collection of vibration signal data, acceleration sensors are placed above the driving end and the fan end to collect the vibration acceleration signal of bearings. The 16 channel data recorder is used to collect vibration signal, and the torque sensor / decoder is used to measure speed and power. The fault bearing is placed on the bearing test bench to obtain the vibration data.

Data Processing

The ball, outer ring and inner ring all have the damage of 0.1778mm, 0.3556mm and 0.5334mm diameters. So the working conditions studied in this paper are as follows: normal state, ball fault 1, ball fault 2, ball fault 3, outer ring fault 1, outer ring fault 2, out ring fault 3, inner ring fault 1, inner ring fault 2 and inner ring fault 3.

In order to preprocess the data, 10001 to 20000 points of data for each condition are selected. The 10000 points were divided into 10 groups with 1000 points in each group. Each group's section s is in equation 1:

$$s = [n, n+999](n = 10001, 11001, \cdots, 19001) \tag{1}$$

where, s is the section of each group, n is the first point of each group. Then each group data is drawn cepstrum. The amplitudes of the four largest peaks of the cepstrum are preserved.

Primitive Cepstrum and Improved Cepstrum Signal Feature in Frequency Domain

According to practical engineering experience, the rotating frequency of bearing inner ring *F_{i}* and the comparative rotating frequency of bearing outer ring and inner ring *F_{io}* are shown in equation 2 to equation 3:

$$F_i = \frac{l}{60} \tag{2}$$

$$F_{io} = F_i - F_o = F_i \tag{3}$$

where, *l* is the speed of bearing inner ring. The comparative rotating frequency of the rolling element and the inner ring *F_{Bi}*, the comparative rotating frequency of the rolling element and the inner ring *F_{Bo}*, the rotation frequency of rolling element relative to bearing center *F_{BB}* are shown in equation. 4 to equation. 6:

$$F_{Bi} = \frac{Q}{2} F_{io}\left(1 + \frac{R_d}{D_d}\cos\beta\right) \tag{4}$$

$$F_{Bo} = \frac{Q}{2} F_{io}\left(1 - \frac{R_d}{D_d}\cos\beta\right) \tag{5}$$

$$F_{BB} = \frac{Q}{2}\left(1 - \frac{R_d}{D_d}\cos\beta\right) \tag{6}$$

where, *Q* is the number of rolling elements, *R_{d}* is the diam of rolling element, *D_{d}* is the pitch diam of rolling elements raceway, and β is the contact angle of bearings. But it is impossible to realize fault identification only from frequency domain, more accurate methods need to be proposed.

Primitive Cepstrum

The definition of cepstrum is shown in equation. 7:

$$C\{x(n)\} = ifft\{\log\{fft(x(n))\}\} \tag{7}$$

where, *x(n)* is the discrete signal sequence, *fft* is fast Fourier transform, *ifft* is inverse Fourier transform, and *C* is cepstrum. The primitive cepstrum is shown in Figure 2.

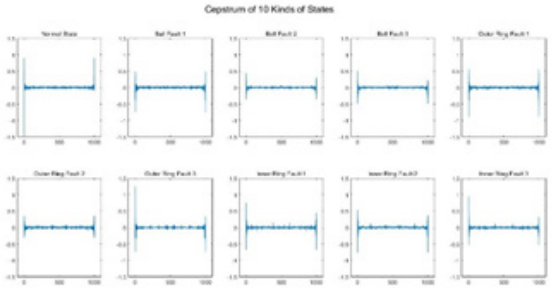

Figure 2: The primitive cepstrum

As shown in Figure 2, the primitive cepstrum has four maximal peak value. The top left peaks, the top right peaks, the bottom left peaks and the bottom right peaks are in turn called PE1, PE2, PE3 and PE4. But all working conditions can't be distinguished only by using the four peaks of cepstrum. Such as ball fault 1 and outer fault 1, inner fault 1 and inner fault 3, which have the same feature so that fault cannot be distinguished. So improved cepstrum is proposed.

Improved Cepstrum

The accuracy of original cepstrum for fault diagnosis is not high, so improved cepstrum is proposed to increase diagnosis accuracy. The improved cepstrum means to find corresponding thresholds to reset the size of four maximal peaks. The flow chart of the improved cepstrum is shown in Figure 3. If the peak is greater than the absolute of corresponding threshold, the peak will be set to 1;

if the peak is less than the absolute of corresponding threshold, the peak will be set to 0. For the interval with serious cross, the blind area is set to ignore cross issues.

In order to find the threshold of the top left peaks, the top left peaks are shown in Figure 4.

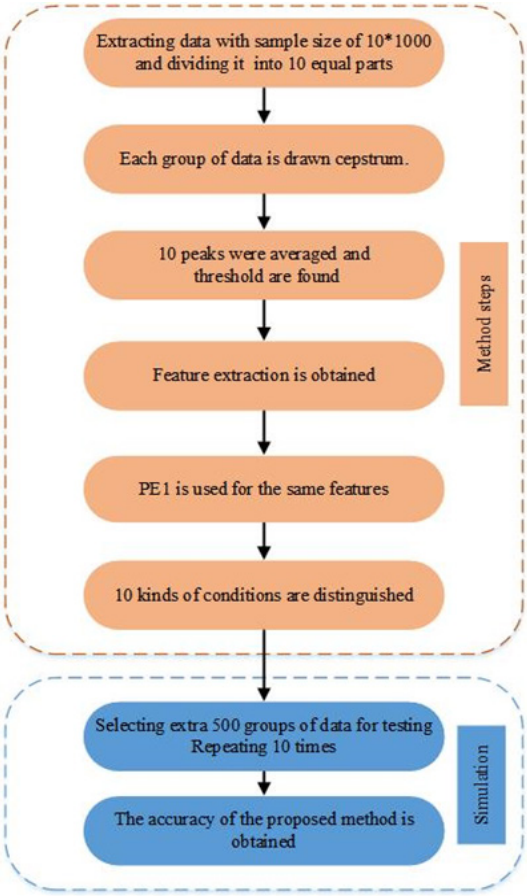

Figure 3: The flow chart of the improved cepstrum

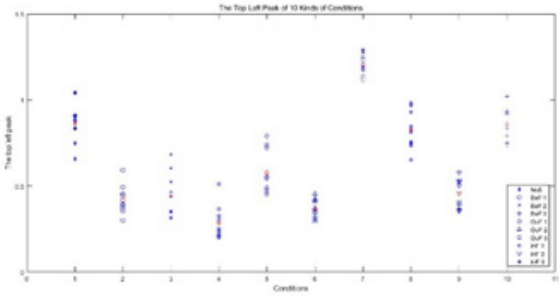

Figure 4: The top left peaks

As shown in Figure 4, the NoS represents the normal state, the BaF represents the ball fault, the OuF represents the outer ring fault and the InF represents the inner ring fault. The blue dots represent the peaks of the cepstrum, and the red dots represent the average of the cepstrum peaks. According to the distribution of the top left peaks, the corresponding threshold range can be found easily. The threshold of top left peaks is in the section [0.57,0.82], so the point 0.7 is selected for the threshold of top left peaks. The threshold of the top left peaks is found. In order to find the threshold of the top right peaks, the top right peaks are shown in Figure 5.

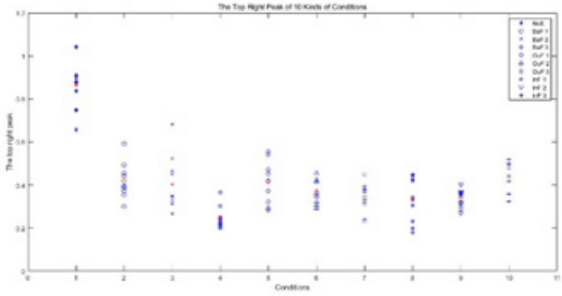

Figure 5: The top right peaks

As shown in Figure 5, the NoS represents the normal state, the BaF represents the ball fault, the OuF represents the outer ring fault and the InF represents the inner ring fault. The blue dots represent the peaks of the cepstrum, and the red dots represent the average of the cepstrum peaks. According to the distribution of the top right peaks, the corresponding threshold range can be found easily. The threshold of top right peaks is in the section [0.33,0.38], so the point 0.332 and 0.378 are selected for the threshold of top right peaks, and the section [0.332, 0.378] is blind area, not judged. The threshold of the top right peaks is found. In order to find the threshold of the bottom left peaks, the bottom left peaks are shown in Figure 6.

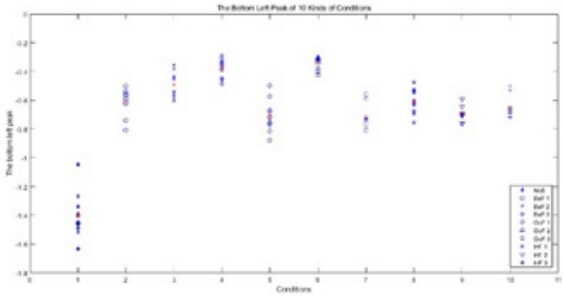

Figure 6: The bottom left peaks

As shown in Figure. 6, the NoS represents the normal state, the BaF represents the ball fault, the OuF represents the outer ring fault and the InF represents the inner ring fault. The blue dots represent the peaks of the cepstrum, and the red dots represent the average of the cepstrum peaks. According to the distribution of the bottom left peaks, the corresponding threshold range can be found easily. The threshold of bottom left peaks is in the section [-0.61,-0.49], so the point -0.6 and -0.52 are selected for the threshold of bottom left peaks, and the section [-0.6, -0.52] is blind area, not judged. The threshold of the bottom left peaks is found. In order to find the threshold of the bottom right peaks, the bottom right peaks are shown in Figure 7.

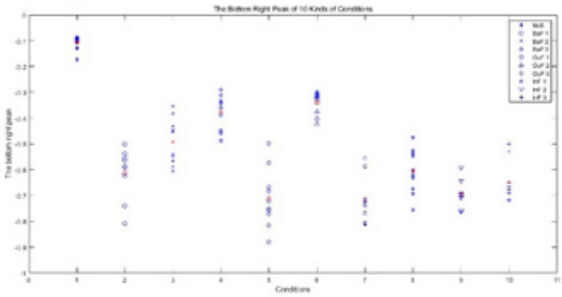

Figure 7: The bottom right peaks

As shown in Figure 7, the NoS represents the normal state, the BaF represents the ball fault, the OuF represents the outer ring fault and the InF represents the inner ring fault. The blue dots represent the peaks of the cepstrum, and the red dots represent the average of the cepstrum peaks. According to the distribution of the bottom right peaks, the corresponding threshold range can be found easily. The threshold of bottom right peaks is in the section [-0.5, -0.37], so the point -0.447 is selected for the threshold of bottom right peaks. The threshold of the bottom right peaks is found.

So far, all four peaks have been found. The detailed use criteria of threshold are as follows:
For the top left peak: if the absolute of average peak is greater than 0.7, the peak will be set to 1; if the absolute of average peak is less than 0.7, the peak value will be set to 0. Do not include page numbers in the text.

For the top right peak: if the absolute of average peak is greater than 0.378, the peak will be set to 1; if the absolute of average peak is less than 0.332, the peak will be set to 0; [0.332, 0.378] is dark area, if the absolute of average peak is in this section, the peaks will be not judged.

For the bottom left peak: if the absolute of average peak is greater than 0.6, the peak will be set to 1; if the absolute of average peak is less than 0.52, the peak will be set to 0; [0.52, 0.6] is dark area, if the absolute of average peak is in this section, the peaks will be not judged.

For the bottom right peak: if the absolute of average peak is greater than 0.447, the peak will be set to 1; if the absolute of average peak is less than 0.447, the peak will be set to 0.

The theoretical feature extraction graph can be inferred by using the four thresholds. Then the theoretical feature extraction is shown in Figure 8.

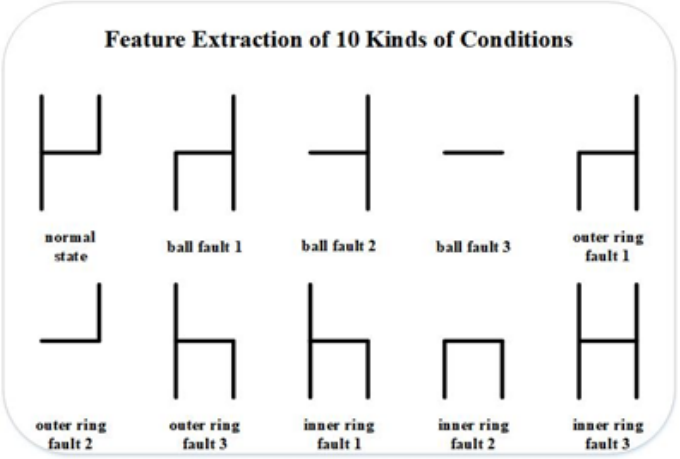

Figure 8: Feature extraction based on improved cepstrum

The features of each working condition are extracted in Figure. 8, each peak has only 2 values: 1 or 0. And each condition has a specific feature, but the same feature between different working conditions are still existing, such as BaF1 and OuF1. So a supplementary criterion is proposed to solve the problem of same feature. The top left peak *PE1* is used to further distinguish the same features. The supplemental principles are as follows:

For the outer ring fault 1 and the ball fault 1: if *PE1* is greater than 0.48, the fault will be outer ring fault 1; if *PE1* is less than 0.48, the fault will be ball fault 1.

For the outer ring fault 3 and the inner ring fault 1: if PE1 is greater than 1, the fault will be outer ring fault 3; if PE1 is less than 1, the fault will be inner ring fault 1.

After the provisions of supplementary criterion, 10 kinds of conditions are distinguished totally. Each working condition has its own feature. Simulation experiment is designed and carried out in following section.

Simulation Experiment

In order to verify the effectiveness of the improved cepstrum method, more data that cut from point 60001 of each state to point 120000 are selected. The data of each condition has 60000 points, which form a column. And 10 kinds of conditions data form a matrix G. The matrix T has 60000 lines, 10 columns, and the arrangement of 10 kinds of conditions is the same as Fig. 4. The matrix G is shown in equation. 8:

$$G(a_1,\ldots,a_k,b_1,\ldots,b_m)=\begin{bmatrix} a_1b_1 & \cdots & a_1b_m \\ \vdots & \ddots & \vdots \\ a_kb_1 & \cdots & a_kb_m \end{bmatrix}_{k\times m} \quad (8)$$

where, k=60000, m=10. Select 10 groups of continuous 1000 discrete points of any column from the matrix G, then 10 groups of data were drawn cepstrum and take the largest four peaks. Ten peaks at the same location are averaged, then the average is compared with the threshold value, so that the average peaks are set to 1 or 0. Therefore, actual features are obtained. If actual features are the same as theoretical features in section 3.2 and meet the condition of the top left peak *PE1,* correct times will plus one. The same process was repeated 500 times. The accuracy is shown in equation 9:

$$A_{cc}=\frac{P}{T} \quad (9)$$

where, *A_{cc}* is accuracy, *P* is correct times and *T* is The number of experiments. Recording the running time at the same time. In this way, the accuracy and running time is shown in Tables 1.

Table 1: Accuracy and Running time

Group	Accuracy	Running time/s
Group1	92.80%	0.8627
Group2	93.20%	0.7805
Group3	92.60%	0.7697
Group4	92.40%	0.8797
Group5	93.60%	0.8283
Group6	91.60%	0.8954
Group7	92.80%	0.8416
Group8	91.40%	0.8641
Group9	90.40%	0.7465
Group10	93.60%	0.8630
Average	92.44%	0.8332

As shown in Tables 1, the accuracy of the proposed method has been up to 92.44% and proved the effectiveness. Therefore, the new method proposed in this paper is feasible. It is reasonable to believe that this method will be applied in the future.

Conclusion

In this paper, a new method based on improved cepstrum for bearing fault diagnosis is proposed. The four largest peaks of the cepstrum are extracted and improved by using corresponding threshold. The search of threshold is completed by studying the peak graph. The result shows the accuracy of the proposed method is up to 92.44%, which has proven the feasibility of the method. In the follow study, to get higher accuracy and smaller blind area, furthermore research should be carried out. It is believed that the research will have a good application prospect.

References

1. Karatoprak, E., & Seker, S. (2019). An improved empirical mode decomposition method using variable window median filter for early fault detection in electric motors. Mathematical Problems in Engineering, 2019.
2. Zheng, J., & Pan, H. (2020). Mean-optimized mode decomposition: An improved EMD approach for non-stationary signal processing. ISA transactions, 106, 392-401.
3. He, C., Niu, P., Yang, R., Wang, C., Li, Z., & Li, H. (2019). Incipient rolling element bearing weak fault feature extraction based on adaptive second-order stochastic resonance incorporated by mode decomposition. Measurement, 145, 687-701.
4. Cai, G., Yang, C., Pan, Y., & Lv, J. (2019). EMD and GNN-AdaBoost fault diagnosis for urban rail train rolling bearings. Discrete & Continuous Dynamical Systems-S, 12(4&5), 1471.
5. Wang, C., & Gan, M. (2019). A supervised sparsity-based wavelet feature for bearing fault diagnosis. Journal of Intelligent Manufacturing, 30(1), 229-239.
6. Li, H., Liu, T., Wu, X., & Chen, Q. (2019). Enhanced frequency band entropy method for fault feature extraction of rolling element bearings. IEEE Transactions on Industrial Informatics, 16(9), 5780-5791.
7. Wan, S., & Peng, B. (2019). The FERgram: A rolling bearing compound fault diagnosis based on maximal overlap discrete wavelet packet transform and fault energy ratio. Journal of Mechanical Science and Technology, 33(1), 157-172.
8. Chen, B., Shen, B., Chen, F., Tian, H., Xiao, W., Zhang, F., & Zhao, C. (2019). Fault diagnosis method based on integration of RSSD and wavelet transform to rolling bearing. Measurement, 131, 400-411.
9. Huang, L., Huang, H., & Liu, Y. (2019). A Fault Diagnosis Approach for Rolling Bearing Based on Wavelet Packet Decomposition and GMM-HMM. International Journal of Acoustics & Vibration, 24(2).
10. Zhang, X., Zhu, J., Wu, Y., Zhen, D., & Zhang, M. (2020). Feature Extraction for Bearing Fault Detection Using Wavelet Packet Energy and Fast Kurtogram Analysis. Applied Sciences, 10(21), 7715.
11. Wei, D., Jiang, H., Shao, H., Li, X., & Lin, Y. (2019). An optimal variational mode decomposition for rolling bearing fault feature extraction. Measurement Science and Technology, 30(5), 055004.